Fachtagung "Experimentelle Strömungsmechanik"
5.–7. September 2023, München

Strömungsfeldanalyse eines Hubschrauber Windkanalmodels mit unterschiedlichen Blattstummellängen

Flow Field Analysis on a Helicopter Wind Tunnel Model with Varying Blade Stub Lengths

Ulrich Hartmann, Christian Breitsamter
Chair of Aerodynamics and Fluid Mechanics
TUM School of Engineering and Design
Technical University of Munich
Boltzmannstr. 15
D-85748 Garching bei München

Hubschrauber, Rotornachlauf, Blattstummel, Windkanal
helicopter, rotor wake, blade stubs, wind tunnel

Zusammenfassung / Summary

Aerodynamische Kraft- und Strömungsfeldmessungen wurden an einem skalierten Hubschraubermodell im Maßstab 1:7.33 durchgeführt. Insbesondere wird dabei die Ausführung des Rotorkopfes betrachtet. Drei verschiedene Rotorkopfvarianten mit unterschiedlicher Blattstummellänge wurden untersucht. Zusätzlich variierte die Anstellung der Blätter von einer fixen Rotorposition, zu kollektiver und zyklischer Blattverstellung. Bei den längsten Blattstummeln sind größere Unterschiede im Auftriebs- und Nickmomentenkoeffizient erkennbar. Das Strömungsfeld direkt hinter dem Rotorkopf unterscheidet sich nicht signifikant zwischen den verschiedenen Blatteinstellungen, jedoch sind ausgeprägte Blattspitzenwirbel bei der fixen Konfiguration erkennbar. Bei den mittleren Blattstummeln ist der Kraftunterschied zwischen fixer und kollektiver Blatteinstellung geringer. Der Einfluss der zyklischen Blattverstellung spiegelt sich vor allem im Auftrieb und Nickmoment wider. Die Kräfte der kleinsten Blattstummel ähneln denen am fixierten Rotor mit mittleren Blattstummellängen.

Experimental investigations using aerodynamic force and flow field measurements have been performed on a 1:7.33 scaled helicopter model in the wind tunnel with special focus on the rotor head. Three rotor head configurations with varying blade stub lengths, so-called largest, medium and short, are analyzed. In addition, the rotor head movement is varied from a fixed rotor head to collective and cyclic pitch movement. The largest blade stubs differ in the lift and pitching moment coefficient, especially for the cyclic rotation. Behind the hubcap, the flow field looks overall similar between these configurations, while tip vortices are identified clearly for the fixed approach. The medium blade stubs show less deviation between the fixed and collective movement, while cyclic rotational movement influences the lift and pitching moment coefficient the most. The wake structure does not show significant variations behind the hubcap between these configurations. The aerodynamic forces and the flow field of the shortest blade stubs resemble the one for the fixed medium blade stub lengths.

GALA e.V., Karlsruhe, Germany, ISBN 978-3-9816764-9-5

Introduction

Experiments on helicopters are mainly carried out on scaled and simplified models. However, most helicopter rotors are too big to fit into classical wind tunnels. In addition, the relevant Mach and Reynolds effects can not be depicted on scaled helicopter rotor models. Therefore, the rotor blades are truncated, while the aerodynamic characteristics of the fuselage, tail boom, and horizontal and vertical tail are investigated in wind tunnel experiments. Using blade stubs can lead to unintentional interactional effects, as the tip vortices are closer to the main body than for full helicopter blades. There is no clear guideline to shape the blade stubs, and different approaches are found in the literature.

Therefore, this study investigates the influence of the rotor head with varying blade stub lengths on the aerodynamic behavior of the helicopter. Interactional aerodynamics between the main and tail rotor were investigated by Sheridan [1]. Reich et al. [2,3,4] and Shenoy et al. [5] investigated the drag and flow phenomena around different generic rotor hubs. Previous experimental and numerical investigations were conducted at the Chair of Aerodynamics and Fluid Mechanics of the Technical University of Munich (TUM) by [6,7,8].

Experimental Setup

The experiments have been carried out at the low-speed wind tunnel facility A of the Chair of Aerodynamics and Fluid Mechanics of TUM. The test section has a height of 1.8 m, a width of 2.4 m, and a length of 4.8 m, and the experiments have been conducted at an open test section. The turbulence level of the wind tunnel facility is below 0.4%, and the maximum uncertainty in the spatial and temporal mean velocity distribution is 0.67%.

The experiments have been performed on a 1:7.33 scaled helicopter model of a characteristic twin-engine light (TEL) utility helicopter, which consists of the fuselage, skid landing gear, mast fairing, rotor head, tail boom, and horizontal and vertical tail. The empennage is positioned in a T-tail arrangement. Figure 1 shows the helicopter model in the wind $_{\text{tunnel}}$ test section mounted on a tail sting support.

Figure 1: Helicopter Model in the Wind Tunnel with Rotor Head R1

Figure 2: Rotor Head Variants: R1 (left), R2 (middle), and R3 (right)

In this study, three varying blade stub lengths are investigated and displayed in Fig. 2. The longest blade stubs, namely R1, are shown on the left part of the figure and also in the wind tunnel model. In relation to the hubcap diameter, the blade length is approximately twice of this diameter. In the middle, rotor head variant R2 is depicted, while the smallest blade stub length is shown on the right side. The blade length of R2 resembles the diameter of the hubcap, and the blade length to hubcap ratio of 0.4 is given by variant R3.

GALA e.V., Karlsruhe, Germany, ISBN 978-3-9816764-9-5

During the experiments, aerodynamic forces and moments are recorded by a six-component underfloor balance system, and the wake flow field of the rotor heads is captured by stereo particle image velocimetry (PIV) measurements. The measurement range of the balance in the axial direction is F_x = +-1500 N, while in horizontal and vertical directions $F_y = F_z$ = +-3000 N. The moment measurement range spans $M_x = M_z$ = +-700 Nm and M_y = +-500 Nm. The six-component system has an accuracy based on maximum loads of 0.025% for the force and moment components. The resulting maximum uncertainties for the force coefficients are below 5.7 x 10^{-3} and for the moment coefficient 3.5 x 10^{-3}.
The PIV system is mounted outside the test section on a three-axis traversing system, allowing to record cross flow planes on the beginning of the tail boom. A double-pulsed Nd:YAG laser with a maximum power of 325 mJ per pulse and a wavelength of 532 nm illuminates seeding particles (DEHS) with a diameter of approximately 1 x 10^{-3} mm, which circulate in the wind tunnel. The flow field has been captured by two sCMOS cameras with a resolution of 2560x2160 pixels, resulting in a spatial resolution of approximately 1.5 x 10^{-3} m. The sampling frequency of the PIV system was not adapted to a specific blade position, leading to time-averaged flow field measurements. In total, 400 images per section were recorded. The uncertainties of the mean velocity components are quantified to $|u_{err} / U_{inf}| = |v_{err} / U_{inf}| = |w_{err} / U_{inf}| < 0.015$ [9]. The initial interrogation window is set to 48x48 pixels with 50% overlap, and the final to 32x32 pixels and 75% overlap by four passes.

Flow Field Analysis of Rotor Head R1

The resulting aerodynamic forces and moments of the different helicopter configurations with rotor head R1 are listed in Tab. 1. The first line displays the forces for the fixed blade position, where one blade faces in the forward direction. Between the second and third lines, the type of rotor movement varies. The second line reports the forces for a rotating rotor head with a constant pitch angle, and it is stated as the collective rotor head configuration. For the third line, the rotor performs a cyclic pitch movement.

	C_x	C_y	C_z	C_l	C_m	C_n
FVH+R1-fix	0.358	0.069	-0.042	-0.042	-0.115	0.426
FVH+R1-coll	0.329	0.067	0.145	-0.048	-0.097	0.514
FVH+R1-cyl	0.339	0.069	0.084	-0.012	-0.107	0.469

Table 1: Aerodynamic Forces and Moments of Rotor Head R1

Minor differences between the fixed, collective and cyclic approaches are detected for the drag and side force coefficients. The rotor rotation leads to a decrease in drag and in the side force. In addition, adding rotation to the longest blade stubs significantly increases the lift coefficient as the profiled blades generate lift. Thereby, the lift for the collective rotation increases more than for the cyclic one. The fixed rotor head and the collective rotation lead to a similar rolling moment coefficient. The rolling moment coefficient decreases for the cyclic rotation as the inclination of the tip path plane counterbalances the asymmetrical inflow conditions on the advancing and retreating blade sides. Applying the rotation increases the pitching and yawing moment, whereby the collective rotation results in the largest values.
The rotor wake is captured at a cross flow plane at the beginning of the tail boom for all three rotor head configurations. Figure 3 shows the axial velocity component (a), vertical velocity component (b), and axial vorticity (c) of the rotor head with the longest blade stubs (R1) for the fixed (left), collective (middle), and cyclic movement (right).

GALA e.V., Karlsruhe, Germany, ISBN 978-3-9816764-9-5

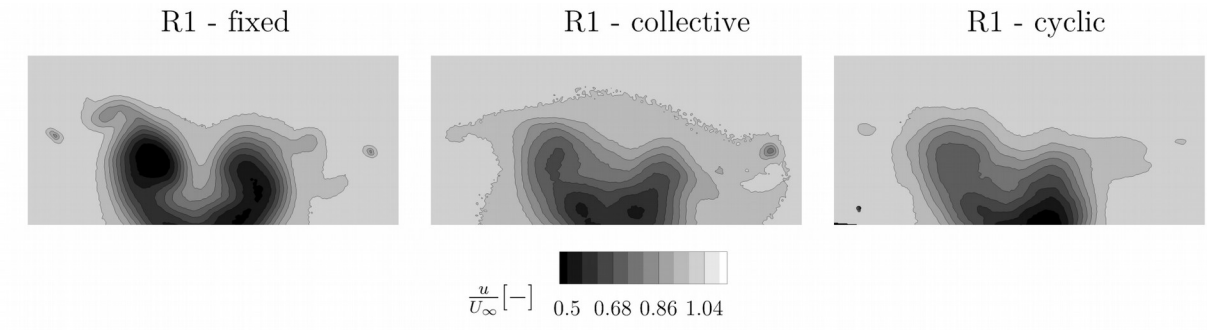

a) Axial Velocity Component

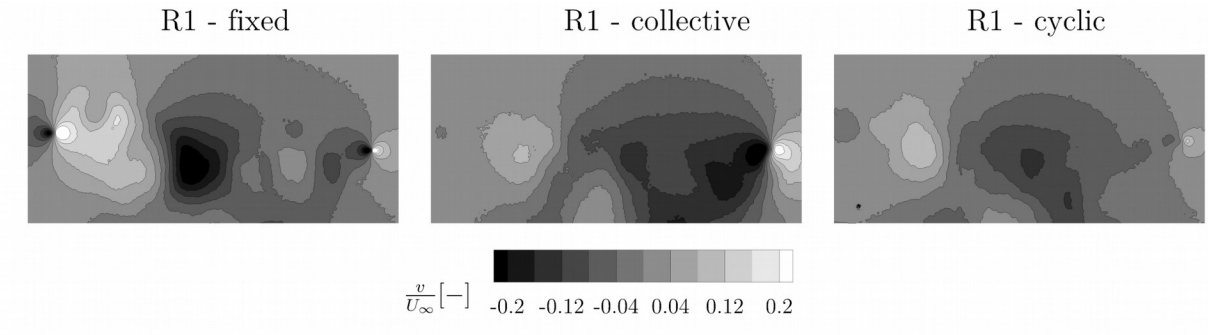

b) Vertical Velocity Component

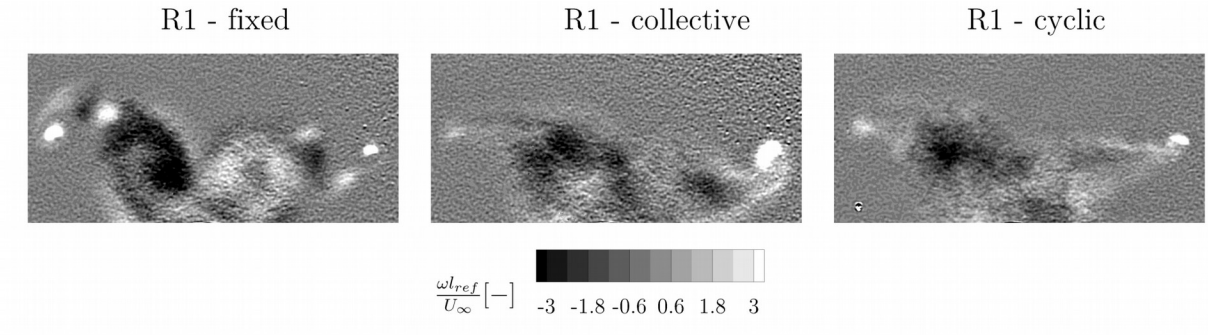

c) Axial Vorticity Component

Figure 3: Cross Flow Planes of Rotor Head R1

First, the axial velocity component (Fig. 3a) is analyzed. The flow field consists of two velocity deficit areas located behind the hubcap. The fixed rotor head approach separates these velocity areas into the advancing and retreating blade side parts. Applying rotation decreases the velocity deficit area, especially the region with pronounced velocity reduction, and the flow parts of the retreating and advancing sides are combined. The largest velocity deficit area is detected for the fixed configuration, consistent with the highest drag coefficient given in Tab. 1. The asymmetry in the collective and cyclic rotor's flow field results from the different blade orientations of the advancing and retreating blades. For the fixed rotor head, two velocity drop spots are detected on the advancing and retreating blade side, which are linked to the blade tip vortices. Only one distinct tip vortex is noticed on the advancing blade side for the collective blade movement. For the cyclic rotor blades, no distinct drops are detected in the axial velocity flow field. Due to the rotating blades, the blade tip vortices move vertically and horizontally, leading to smearing out of these distinct velocity areas.
The vertical velocity component is shown in Fig. 3b. The centrally located area with negative velocity is linked to the hubcap's downwash. On the retreating blade side, an upward velocity component results from the rear inflow of the blades. This positive velocity area is the largest

GALA e.V., Karlsruhe, Germany, ISBN 978-3-9816764-9-5

for the fixed approach, while its size decreases for the collective and cyclic rotation. The contrary-orientated velocity field on the advancing blade side results from the tip vortex. For the collective rotor movement, the downwash area behind the hubcap increases towards the advancing blade side due to the lift generation of the profiled blade. In addition, the flow field of the positive velocity components decreases in size. For the cyclic blade movement, the downwash region further decreases in size while the positive velocity component area increases. This behavior coincides with the higher lift coefficients for the collective movement than for the cyclic one.
The non-dimensional vorticity is shown in Fig. 3c. The large area of negative and positive vorticity in the center is connected to the left and right parts of the hubcap vortex pair. Both parts are captured for the fixed rotor head approach, while the right hubcap vortex part is less present in the collective and cyclic approach. Below the hubcap vortex pair, the two counter-rotating vorticity areas originate from the mast fairing vortex pair. Further outwards, spots of high positive vorticity demonstrate the blade tip vortices of the retreating and advancing blades. The fixed rotor head shows two distinct spots on the retreating and advancing blade each, while only one is detected for the collective and cyclic rotation.

Flow Field Analysis of Rotor Head R2
For the medium blade lengths, the resulting aerodynamic forces of the helicopter configurations are shown in Tab. 2.

	C_x	C_y	C_z	C_l	C_m	C_n
FVH+R2-fix	0.314	0.103	-0.016	-0.098	-0.162	0.419
FVH+R2-coll	0.301	0.122	-0.004	-0.101	-0.174	0.485
FVH+R2-cyl	0.289	0.148	-0.059	-0.145	-0.062	0.578

Table 2: Aerodynamic Forces and Moments of Rotor Head R2

Similar to the largest blade stubs of rotor head R1, the rotation decreases the drag coefficient of the helicopter configuration. In contrast to R1, the side force increases for the collective and cyclic movement of the rotor heads. Especially for the cyclic rotation, the side force nearly doubles. The collective rotor head increases the lift coefficient of the helicopter configuration compared to the fixed approach, while the lift decreases for the cyclic movement. The rolling moment of the cyclic rotation is higher than that of the fixed and collective approaches, which is consistent with the increase in side force. The pitching moment of the collective rotation slightly decreases, while it increases significantly for the cyclic one. Adding the rotation leads to an increase in each yawing moment coefficient.
For rotor head R2, the axial velocity component is shown in Fig. 4a.

GALA e.V., Karlsruhe, Germany, ISBN 978-3-9816764-9-5

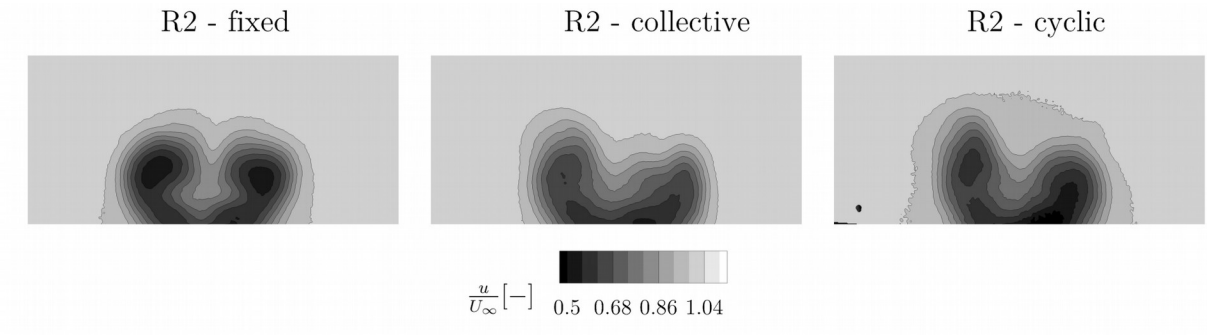

a) Axial Velocity Component

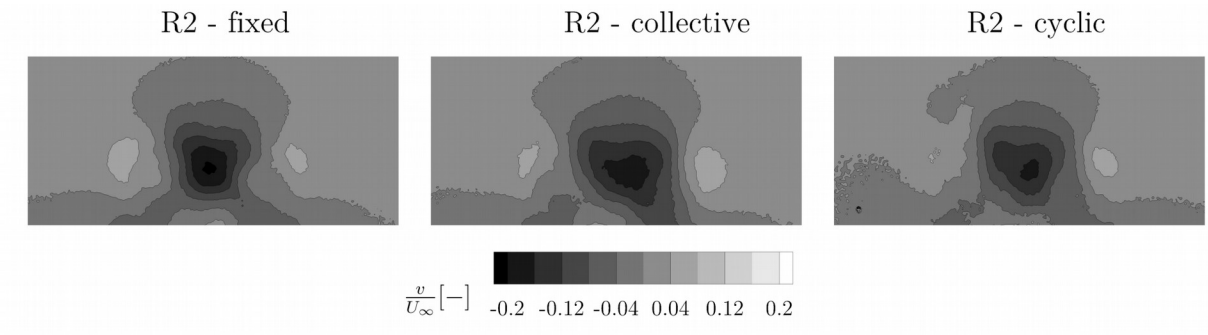

b) Vertical Velocity Component

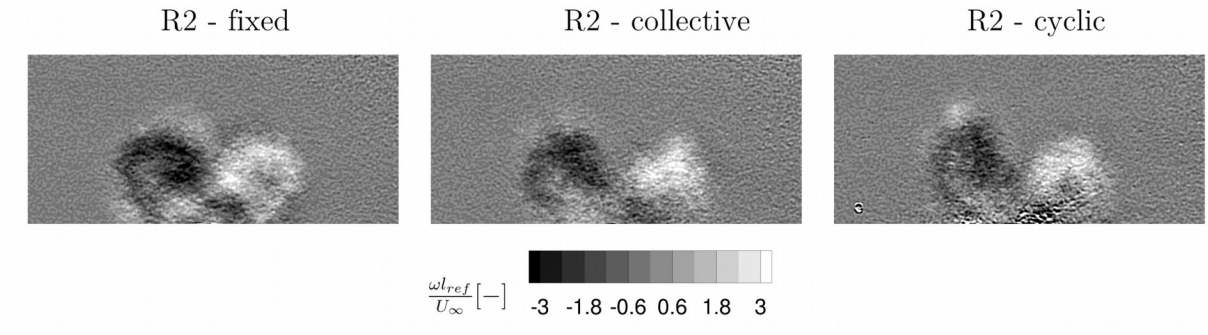

c) Axial Vorticity

Figure 4: Cross Flow Planes of Rotor Head R2

As for rotor head R1, one large velocity deficit area is centrally located behind the hubcap, and the resulting flow field of the fixed rotor head is symmetric. By applying the rotation, the velocity deficit area on the retreating blade side increases vertically, leading to an asymmetric flow structure. The vertical velocity component of rotor head R2 is given in Fig. 4b. For the fixed, collective, and cyclic rotor head, one large area with negative velocity is placed centrally behind the hubcap. This velocity area is connected to the downwash of the hubcap. When the rotation is on, the area slightly increases. In addition, two spots of positive velocity are located on the left and right sides of the hubcap. The axial vorticity fields related to the R2 rotor head are given in Fig. 4c. Two distinct vorticity regions originating from the hubcap vortex pair are shown centrally for the fixed, collective, and cyclic rotor motion. In the fixed approach, both vorticity areas are similar in shape. Additional vorticity regions are detected below the hubcap vortex pair, which are related to the wake of the mast fairing. For the collective rotor head approach, the vorticity region of the retreating blade side decreases slightly in size. In contrast, one additional spot of positive vorticity is detected on the retreating blade side for the cyclic approach.

GALA e.V., Karlsruhe, Germany, ISBN 978-3-9816764-9-5

Flow Field Analysis of Rotor Head R3

For rotor head configuration R3, only the collective movement was investigated in the wind tunnel, and the resulting forces are given in Tab. 3. A force comparison is performed with the previously presented values of rotor head R1 and R2.

The rotor head with the smallest blade stubs provides the lowest drag value compared to all other configurations. The side force, lift, rolling, and pitching moment coefficients are in a similar range to the one from the fixed rotor head R2 configuration. Only the yawing moment of the fixed R1 rotor head is slightly closer to the smallest rotor head approach than the fixed R2 rotor head.

	C_x	C_y	C_z	C_l	C_m	C_n
FVH+R3-coll	0.268	0.109	-0.028	-0.099	-0.184	0.433

Table 3: Aerodynamic Forces and Moments of Rotor Head R3

Figure 5 shows the axial and vertical velocity components and the axial vorticity of rotor head R3 for the collective pitch. The axial velocity component shows two velocity deficit areas, where the one associated with the advancing blade side is larger than the one of the retreating side. This behavior differs from R1 and R2, where the velocity on the left hubcap sides decreases even more. In the vertical velocity component, the downwash of the hubcap is detected. The collective rotation leads to a slight shift to the advancing side on the bottom side of the downwash area. This displacement was also observed for R1 and R2, while the magnitude and displacement were lower for R3. The vorticity flow field shows the hubcap vortex and partly the mast fairing vortex pair. Comparing the aerodynamic forces and the flow field, rotor head R3 with the smallest blade stubs behaves similarly to the fixed rotor head of the medium blade stubs R2.

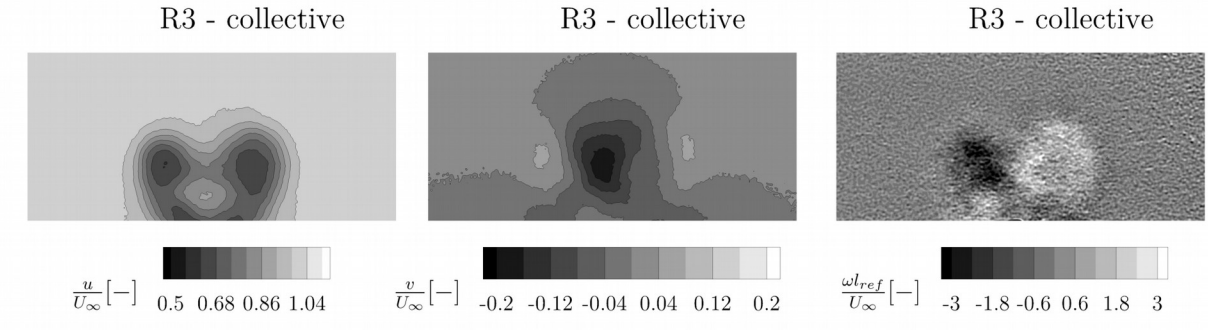

Figure 5: Cross Flow Planes of the Axial Velocity (left), Vertical Velocity (middle), and Axial Vorticity (right) of Rotor Head R3

Conclusion

Aerodynamic forces and moments and cross flow velocity field of three rotor head configurations with varying blade stub lengths are investigated on a 1:7.33 scaled wind tunnel model of a light utility helicopter. In addition, the movement of the rotor head is varied from a fixed rotor head approach to a collective and cyclic one.

The fixed, collective, and cyclic movement of the rotor head with the largest blade stub length provides nearly similar forces and moments, except for the lift and rolling moment. Especially for the cyclic approach, the difference increases. A flow field comparison shows a similar centrally located wake structure for all rotor heads, while in the fixed approach, the tip vortices are distinctly pronounced. A comparison of the medium blade stub length shows similar

GALA e.V., Karlsruhe, Germany, ISBN 978-3-9816764-9-5

aerodynamic forces for the fixed and collective rotor blade settings again, while higher differences, especially for the lift and pitching moment coefficient, occur for the cyclic movement. A flow field comparison showed similar wake structures, where the rotation of the blades leads to an asymmetric flow field. The shortest blade stubs, mounted at rotor head R3 and rotated in a collective manner, show a similar force behavior to the fixed approach from rotor head R2. A slight variation in the flow field is observed between the shortest and medium blade stub length, where the axial velocity component increases more on the advancing side than the medium rotor head R2.
Adding the rotor head is necessary to illustrate the influence of the rotor on the helicopter's characteristics. However, the size and shape of the truncated blades as well as the type of rotation, lead to different flow fields and therefore, different forces and moment characteristics. The effect of moving the rotor heads does not vary significantly for these blade stub lengths. Even though the rotational aspect is not represented by a fixed rotor head approach, the general aerodynamic behavior is captured well. However, the fixed blade position generates more pronounced tip vortices compared to the collective and cyclic pitch.

Acknowledge
The funding of this investigation within the LUFO project NANNY (FKZ: 20Y2109E) by the German Federal Ministry for Economic Affairs and Climate Action (BMWK) is gratefully acknowledged.

Literatur
[1] Sheridan, P. F., and Smith, R. P., "Interactional Aerodynamics - A New Challenge to Helicopter Technology," Journal of the American Helicopter Society, Vol. 25, (1), January 1980, pp. 3–21. DOI: 10.4050/JAHS.25.1.3
[2] Reich, D., Shenoy, R., Smith, M., and Schmitz, S., "A review of 60 years of rotor hub drag and wake physics: 1954–2014," Journal of the American Helicopter Society, Vol. 61, (2), 2016, pp. 1–17. DOI: 10.4050/JAHS.61.022007
[3] Reich, D., Willits, S., and Schmitz, S., "Scaling and Configuration Effects on Helicopter Rotor Hub Interactional Aerodynamics," Journal of Aircraft, Vol. 54, (5), 2017, pp. 1692–1704. DOI: 10.2514/1.C034250
[4] Reich, D., Sinding, K., and Schmitz, S., "Visualization of a helicopter rotor hub wake," Experiments in Fluids, Vol. 59, 2018, pp. 1–12. DOI: 10.1007/s00348-018-2571-7
[5] Shenoy, R., Holmes, M., Smith, M. J., and Komerath, N. M., "Scaling Evaluations on the Drag of a Hub System," Journal of the American Helicopter Society, Vol. 58, (3), 2013, pp. 1–13. DOI: 10.4050/JAHS.58.032002
[6] Grawunder, M., Reß, R., Stein, V., Breitsamter, C., and Adams, N. A., "Validation of a Flow Simulation for a Helicopter Fuselage Including a Rotating Rotor Head," New Results in Numerical and Experimental Fluid Mechanics X: Contributions to the 19th STAB/DGLR Symposium Munich, Germany, 2016.
[7] Stuhlpfarrer, M., Kümmel, A., and Breitsamter, C., "Investigations of Helicopter Wake Flow Including Rotor-Head Motion," Journal of Aircraft, Vol. 55, (5), 2018, pp. 2114–2126. DOI: 10.2514/1.C034689
[8] Hartmann, U., Ruhland, J., and Breitsamter, C., "Wind Tunnel Analysis of Helicopter Aerodynamics Varying Rotor Head Blade Stub Lengths, " New Results in Numerical and Experimental Fluid Mechanics XIV: Contribution to the 23th STAB/DGLR Symposium (in print)
[9] Sciacchitano A., and Wieneke B., "PIV Uncertainty Propagation," Measurement Science and Technology, 2016

GALA e.V., Karlsruhe, Germany, ISBN 978-3-9816764-9-5